ARMY RESEARCH LABORATORY

Position Estimation for Projectiles Using Low-cost Sensors and Flight Dynamics

by Luisa D. Fairfax and Frank E. Fresconi

ARL-TR-5994 **April 2012**

NOTICES

Disclaimers

The findings in this report are not to be construed as an official Department of the Army position unless so designated by other authorized documents.

Citation of manufacturer's or trade names does not constitute an official endorsement or approval of the use thereof.

Destroy this report when it is no longer needed. Do not return it to the originator.

Army Research Laboratory
Aberdeen Proving Ground, MD 21005-5066

ARL-TR-5994 **April 2012**

Position Estimation for Projectiles Using Low-cost Sensors and Flight Dynamics

Luisa D. Fairfax and Frank E. Fresconi
Weapons and Materials Research Directorate, ARL

REPORT DOCUMENTATION PAGE	Form Approved OMB No. 0704-0188

1. REPORT DATE *(DD-MM-YYYY)*	2. REPORT TYPE	3. DATES COVERED (From - To)
April 2012	Final	September 2011

4. TITLE AND SUBTITLE
Position Estimation for Projectiles Using Low-cost Sensors and Flight Dynamics

5a. CONTRACT NUMBER

5b. GRANT NUMBER

5c. PROGRAM ELEMENT NUMBER

6. AUTHOR(S)
Luisa D. Fairfax and Frank E. Fresconi

5d. PROJECT NUMBER

5e. TASK NUMBER

5f. WORK UNIT NUMBER

7. PERFORMING ORGANIZATION NAME(S) AND ADDRESS(ES)
U.S. Army Research Laboratory
ATTN: RDRL-WML-E
Aberdeen Proving Ground, MD 21005-5066

8. PERFORMING ORGANIZATION REPORT NUMBER
ARL-TR-5994

9. SPONSORING/MONITORING AGENCY NAME(S) AND ADDRESS(ES)

10. SPONSOR/MONITOR'S ACRONYM(S)

11. SPONSOR/MONITOR'S REPORT NUMBER(S)

12. DISTRIBUTION/AVAILABILITY STATEMENT
Approved for public release; distribution is unlimited.

13. SUPPLEMENTARY NOTES

14. ABSTRACT
Navigation of gun-launched precision munitions using affordable technologies is investigated. Estimation algorithms were developed to blend flight dynamic models with measurements from inertial sensors and, if available, global positioning system (GPS). The launch and flight characteristics of the unique, gun-launched environment were exploited both in the state estimator and for novel heuristic parameter identification. The algorithm included using low-cost inertial sensor arrays and general GPS availability. Experimental results from guided mortar flights indicate that the algorithm with only inertial sensor measurements yields position errors less than 40 m over a 30-s flight. Position errors from the experiments decrease slightly using loose coupling when GPS is available. Simulations were conducted to assess algorithm performance over a wider range of conditions. These results demonstrate that position errors are less than tens of meters for flight times of interest to munitions. Estimation is intolerant to inertial sensor errors due to the novel manner in which known flight dynamics are used to compensate measurements. Overall, this effort shows that navigation error resulting from a low throughput algorithm using affordable inertial sensors is sufficient to increase system accuracy for munitions.

15. SUBJECT TERMS
guidance navigation and control, GN&C, INS, loosely-coupled GPS-INS, GPS-INS, GPS-denied, MEMS, Kalman filter

16. SECURITY CLASSIFICATION OF:			17. LIMITATION OF ABSTRACT	18. NUMBER OF PAGES	19a. NAME OF RESPONSIBLE PERSON
a. REPORT	b. ABSTRACT	c. THIS PAGE			Luisa D. Fairfax
Unclassified	Unclassified	Unclassified	UU	38	19b. TELEPHONE NUMBER (*Include area code*) 410-306-2104

Standard Form 298 (Rev. 8/98)
Prescribed by ANSI Std. Z39.18

Contents

List of Figures

List of Tables

1. Introduction

The motivation for this effort is low-cost, effective navigation of gun-launched projectiles. Navigation is essential to delivering lethal payloads via precision munitions on a complex, modern battlefield, which can feature challenging terrain and target characteristics as well as poor network connectivity and situational awareness. Indeed, navigation errors are the driver in delivery accuracy of precision munitions (*1*). While technologies have been developed in the past (*2–4*), there is currently only one type classified gun-launched precision munition available to the U.S. Soldier (*5*).

The global positioning system (GPS) has been used to great effect recently for indirect fire applications (*1, 5–8*). Absolute referencing enables precision point-targeting; however, higher update rates would prove useful. Additionally, pushing ephemeris data across the battlefield and hot starting the receiver post-launch is non-trivial. More work can be done to optimize GPS for gun-launched projectiles (e.g., by using projectile flight dynamics in the process model). GPS has known threats and complex terrain reduces satellite availability.

Strap-down inertial sensors offer higher update rates but suffer from drift due to accumulating error during integration from acceleration to position (*9*). Many efforts outside of the gun-launched research community have addressed coupling GPS and inertial measurements to increase overall navigation performance (*10–12*).

Navigation in the unique gun-launched environment is especially challenging. First, gun-launched munitions, unlike manned or unmanned aircraft, are throwaway items that are often used at high volumes. This factor implies that the system must be low cost and easy to use with limited infrastructure by Soldiers in conflicts around the world.

Measurements both on- and off-board the projectile have limited observability of the information pertinent to estimating states required to guide to target. For example, accelerometers and gyroscopes located off the center of gravity of the rigid body can be compensated for in order to obtain acceleration (and ultimately position), but information concerning the angular acceleration and gravity force orientation must be inferred elsewhere.

High launch loads are imparted to the projectile at launch, which limits packaging options to enable survivability. Significant efforts have addressed survivability and performance of components such as electronics and inertial sensors (*13–19*) during gun launch. Moreover, sensor calibrations (especially of micro-electromechanical [MEMs] devices) may not hold after the gun launch event. Timekeeping is essential to GPS; however, the associated jerk encountered at launch by the projectile causes clock drift.

Projectiles feature relatively short flight times. Indirect fire projectiles often remain aloft for over a minute. Small- and medium-caliber direct fire munitions can fly for 1 s or less. Short time of flight limits filter settling time, in-flight calibration, and GPS acquisition.

The flight dynamics of ballistic and maneuvering projectiles is well understood (*20–23*). Spin rates of large-caliber, gyroscopically stabilized projectiles can be around 300 Hz, which introduces significant coupling in the dynamics at high frequencies. Indirect fire is a reasonably accurate ballistic delivery system with circular error probable (CEP) on the order of hundreds of meters at ranges of 20 km. Thus, navigation to within less than ~100 m would likely improve the system accuracy. Control authority does not need to be large to correct for this magnitude of miss distance, which is fortuitous because tube launch limits volume available for a maneuver system (*1*, *8*, *24*). Minor corrections to the ballistic flight to remove ballistic dispersion errors, such as launch velocity or wind disturbances, is called ballistic nudging in the gun-launched community (*25*).

The goal of this work was to develop a position estimator for the unique gun-launched environment using low-cost measurement devices and projectile flight dynamics. An extended Kalman filter (EKF) was developed to blend accelerometer, gyroscope, and GPS measurements with a dynamic model (point-mass with control [PMC]) of maneuvering projectile flight. GPS, if available, was used in a loosely coupled algorithm. An innovative flight dynamic heuristic was proposed, which greatly reduced the position errors. Aiding an inertial navigation system (INS) with dynamics was examined by Koifman and Bar-Itzhack (*26*) in aircraft and by Burchett (*27*) in projectiles. The approach in this report is novel in leveraging heuristic information about the known and minimally varying projectile flight characteristics to significantly improve position estimates.

This report is organized as follows: the EKF algorithm is provided along with the cascaded filtering of both the flight dynamic heuristic parameters and loosely coupled GPS/INS parameters. Experimental results from gun-launched guided flights are presented, which demonstrate that position errors are sufficient to reduce the system CEP of guided projectiles with the present algorithm. Simulations were also conducted that illustrate the algorithm performance over a wider array of conditions.

2. Algorithm

2.1 Overview

An EKF was used to combine dynamic modeling with measurements and parameter identification to obtain the state estimate. A block diagram of the algorithm is shown in figure 1. In-flight input to the algorithm includes inertial measurement units (IMU) composed of triaxial accelerometers and triaxial gyroscopes, attitude and GPS. The algorithm incorporates the effect

of multiple IMUs (or arrays) composed of low-cost MEMs devices to assess the cost-benefit. Attitude is provided using separate techniques. Recent work has demonstrated reasonably accurate attitude using low-cost magnetometers and/or thermopiles, even in the presence of significant disturbances (*28–31*). GPS data are used in the estimator when available. A goal of this study is to assess the navigation performance if GPS were inaccessible or if the cost could be reduced by excluding a gun-hard GPS receiver and antenna from the system.

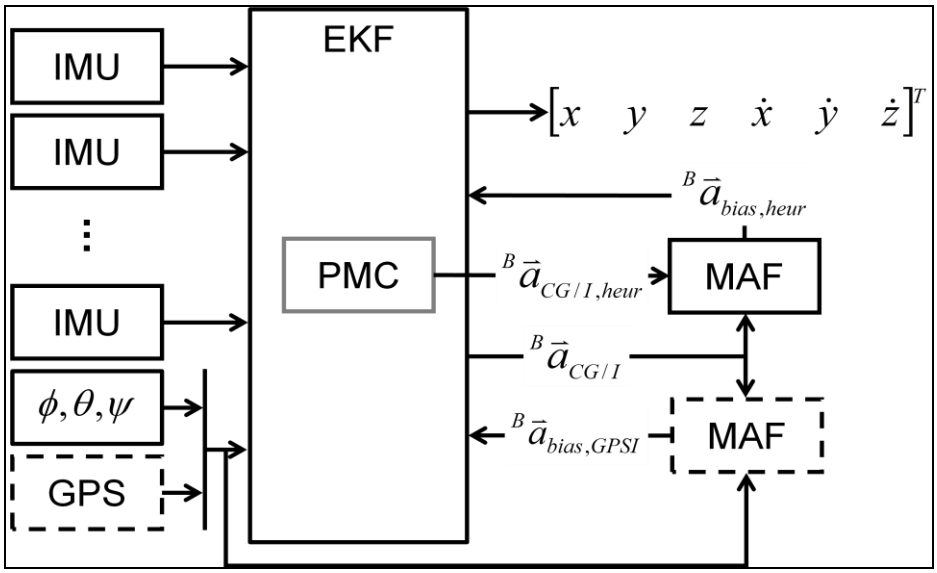

Figure 1. Algorithm block diagram.

A measurement model was formulated to process the raw input. The EKF and moving average filter (MAF) used the PMC flight dynamic model. To accommodate low-cost sensors without prohibitive pre-launch calibration, measurement parameters are estimated in flight with a MAF using flight dynamic heuristics and GPS/INS loose coupling (when the GPS is available). The resulting states estimated by the EKF are inertial position and velocity.

The reference frames of interest are illustrated in figure 2. The standard aerospace sequence for Euler angles relates the body and inertial frames. Gun target line coordinates are used throughout for the inertial frame where the origin is at the gun and the *x*-axis is along the line between the gun and target, the *z*-axis is down, and the *y*-axis completes a right-hand system.

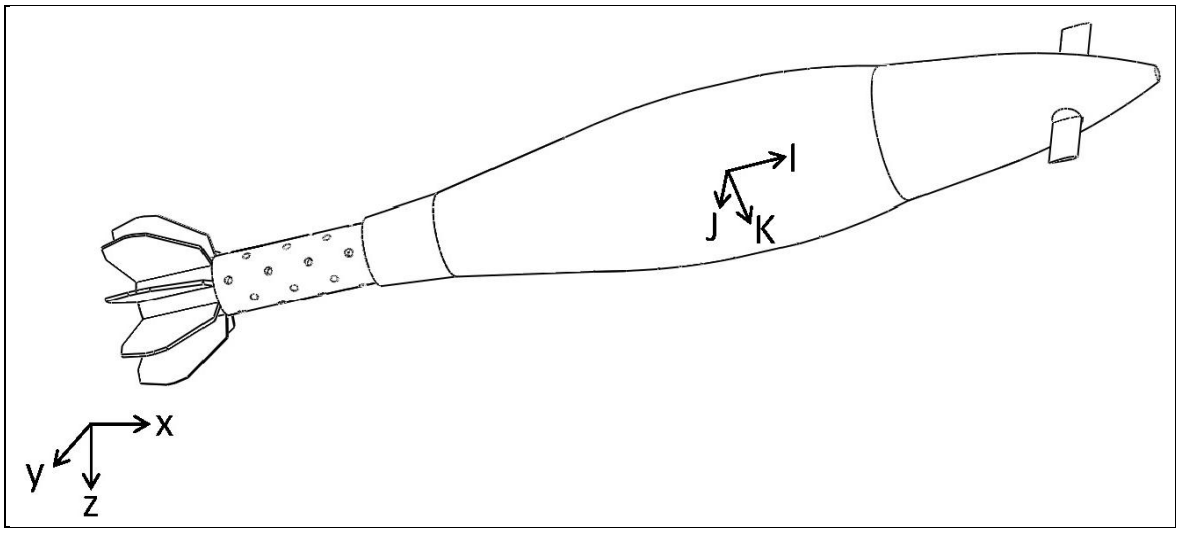

Figure 2. Inertial (x-y-z) and body (I-J-K) reference frames.

2.2 Flight Dynamic Model

The guided projectile concept used for this investigation was a canard-controlled, rolling, fin-stabilized airframe. The point-mass dynamic model represents ballistic projectile flight well (*25*). Maneuvering flight dynamics can be modeled through a control force. For this application, lift of the combined body-fin and roll-averaged lift of the canards is present. These lift terms were added along with the drag and gravity forces typically included in the point-mass dynamic model. Attitude is necessary to resolve the control force components into the inertial frame. Canard direction and magnitude come from onboard guidance calculations (*1*).

The components of acceleration from the nonlinear PMC flight dynamic model are provided in equations 1–3.

$$\ddot{x} = \frac{-\pi C_D d^2 \rho V_\infty}{8m}\dot{x} + \left(c\phi c\psi s\theta + s\phi s\psi\right)\frac{\left(L_{CAN} + L_B\right)}{m} \tag{1}$$

$$\ddot{y} = \frac{-\pi C_D d^2 \rho V_\infty}{8m}\dot{y} + \left(c\phi s\psi s\theta - s\phi c\psi\right)\frac{\left(L_{CAN} + L_B\right)}{m} \tag{2}$$

$$\ddot{z} = \frac{-\pi C_D d^2 \rho V_\infty}{8m}\dot{z} + g + \left(c\phi c\theta\right)\frac{\left(L_{CAN} + L_B\right)}{m} \tag{3}$$

The lift expressions are given in equations 4 and 5. Average angle-of-attack is a function of the inherent maneuverability of the airframe. This term is computed offline from a six degree-of-freedom (6DOF) model. Maximum canard deflection was 10° for this application.

$$L_{CAN} = \frac{-d^2\left(2\delta\cos(\phi_{CAN}) + \pi\alpha\right)\rho C^{C}{}_{L\alpha} V_\infty{}^2}{8} \tag{4}$$

$$L_B = \frac{-\pi d^2 \alpha \rho C^B{}_{L\alpha} V_\infty{}^2}{8} \tag{5}$$

2.3 Measurement Model

A strap-down IMU senses body angular velocity and body acceleration without gravity. In order to get inertial position and velocity, the raw accelerometer and gyroscope output must be expressed as acceleration at the center of gravity (CG) (*9*). The position from the CG to the accelerometer and the body angular acceleration are also required, as shown in equation 6.

$${}^B\vec{a}_{CG/I} = {}^B\vec{a}_{A/B} - \vec{\omega}_{B/I} \times \vec{\omega}_{B/I} \times \vec{r}_{CG\to A} - \vec{\alpha}_{B/I} \times \vec{r}_{CG\to A} \tag{6}$$

The body acceleration of the CG is transformed into the inertial frame and the force of gravity is added as shown in equation 7.

$${}^I\vec{a}_{CG/I} = \vec{T}_{B/I}\,{}^B\vec{a}_{CG/I,comp} + \vec{g} \tag{7}$$

If arrays of IMUs are used, then the resulting inertial acceleration of each IMU is averaged to form a composite inertial acceleration.

Simple Euler integration is applied to obtain velocity and position from the acceleration, as shown in equations 8 and 9.

$${}^I\vec{v}_{k+1} = {}^I\vec{v}_k + {}^I\vec{a}_{CG/I}\,dt \tag{8}$$

$${}^I\vec{x}_{k+1} = {}^I\vec{x}_k + {}^I\vec{v}_{k+1}\,dt \tag{9}$$

As a result of this integration, velocity and position error accumulate over time, and this error is known as INS drift. INS drift can be so large for strap-down MEMs sensors that measurements are quickly not useful for state estimation. This work greatly mitigates the drift problem by estimating error parameters.

2.4 Heuristic Parameter Estimation

MEMs sensors are low cost but suffer from large bias, scale factor, misalignment, and misposition errors. Careful calibration reduces these errors but at an increased cost.

Projectiles launched from guns have well-understood ballistic characteristics. For example, a 100-lb round launched at Mach 2.5 does not deviate much from a known trajectory in the absence of any control maneuvers (especially in the first few seconds). This knowledge of the flight dynamics is incorporated in this work to form an innovative heuristic that mitigates the measurement error and greatly improves states estimates.

Nominal mass properties, aerodynamics, and launch conditions can be used to estimate components of the body acceleration of the CG without gravity, as shown in equation 10. It is assumed that the only significant force is drag acting along the axial direction.

$$ {}^{B}\vec{a}_{CG/I,heur} = \begin{bmatrix} \frac{-\pi\rho V_{\infty}{}^{2} d^{2} C_{D}}{8m} & 0 & 0 \end{bmatrix}^{T} \tag{10} $$

Prediction of the body acceleration of the CG without gravity is compared to the measurement calculations to form a measurement bias error, as shown in equation 11. Bias error is the largest source of accelerometer error in this application. Consequently, it is directly modeled in this method. However, this heuristic-based bias error estimate includes all error sources (e.g., flight dynamic modeling, wind, physical tolerances, bias, and scale factor and misalignment of accelerometer and gyroscope). This modeling approach assumes that a bias-type error accounts for all these different error sources, which the results will bear out.

$$ {}^{B}\vec{a}_{bias,heur,k} = {}^{B}\vec{a}_{CG/I} - {}^{B}\vec{a}_{CG/I,heur} \tag{11} $$

A simple moving average filter was used to smooth the heuristic bias, as demonstrated in equation 12. Heuristic bias is primarily estimated during the predictable, ballistic beginning portion of flight and is then used to correct the body acceleration throughout flight.

$$ {}^{B}\vec{a}_{bias,heur} = \rho_{heur}\, {}^{B}\vec{a}_{bias,heur,k-1} + (1-\rho_{heur})\, {}^{B}\vec{a}_{bias,heur,k} \tag{12} $$

2.5 GPS/INS Loose-coupling Parameter Estimation

If GPS is available, it is used as a measurement update in the EKF (*32*). Additionally, an acceleration bias can be calculated to further correct the INS by comparing the INS and GPS acceleration values. This is done by first calculating the GPS acceleration by numerically differentiating the current and previous GPS velocities, as shown in equation 13.

$$ {}^{I}\vec{a}_{CG/I,GPS} = \frac{{}^{I}\vec{v}_{GPS,k} - {}^{I}\vec{v}_{GPS,k-1}}{dt_{GPS}} \tag{13} $$

The GPS/INS bias parameter is then calculated by transforming the GPS-derived acceleration and subtracting from the estimated body acceleration without gravity as shown in equation 14. Calculating the GPS/INS bias parameter in the body frame provides a fairly constant value for smoothing and enables this parameter to be used even after GPS is lost.

$$ {}^{B}\vec{a}_{bias,GPSI} = {}^{B}\vec{a}_{CG/I} - \vec{T}_{I/B}\, {}^{I}\vec{a}_{CG/I,GPS} \tag{14} $$

The GPS/INS bias parameter is smoothed using a moving average filter, as shown in equation 15.

$$ {}^{B}\vec{a}_{bias,GPSI} = \rho_{GPSI}\, {}^{B}\vec{a}_{bias,GPSI,k-1} + (1-\rho_{GPSI})\, {}^{B}\vec{a}_{bias,GPSI,k} \tag{15} $$

2.6 Extended Kalman Filter

A sequential EKF was used to combine the modeling, measurements, and parameter estimation. The sequential EKF requires the measurement noise to be modeled as uncorrelated, but a matrix inverse is not required. Furthermore, this approach adapts according to what measurements are available, which is useful when measurements have a varying update rate or drop out during flight.

The EKF propagates the dynamic model at each update. Analytical expressions for the state transition matrix were obtained by linearization of the PMC dynamic model. This matrix was recalculated at each update of the algorithm for propagation of the states and covariance (*33*). The steps for the sequential EKF algorithm are as follows. First, the state is updated, as shown in equation 16.

$$X_k = A_{k-1} X_{k-1} \tag{16}$$

Then, the covariance is propagated forward in time, as demonstrated in equation 17.

$$P_k = A_{k-1} P_{k-1} A_{k-1} + Q_{k-1} \tag{17}$$

When measurements from the IMU or GPS are available, the Kalman gain, state estimate, and covariance are updated, as shown in equations 18–20. Each measurement is used to update the state one at a time. When GPS is available, the INS drift is mitigated by weighting the IMU less and the GPS more as flight time increases. This tuning takes place by adjusting the measurement noise matrix, *R* during flight. For each available measurement $i = 1, ..., r$, where r is the total number of measurements, the following steps are performed.

$$K_{ik} = \frac{P_{i-1,k} C_{ik}^{\ T}}{C_{ik} P_{i-1,k} C_{ik} + R_{ik}} \tag{18}$$

$$X_{ik} = X_{i-1,k} + K_{ik} (Y_{ik} - C_{ik} X_{i-1,k}) \tag{190}$$

$$P_{ik} = (I - K_{ik} C_{ik}) P_{i-1,k} \tag{20}$$

The measurement matrix for this problem is the identity matrix. GPS directly provides the inertial velocity and position. The nonlinear computations from sensed acceleration and angular rate to inertial velocity and position are performed. The compensated body acceleration of the CG without gravity that eventually gets used as the measurement is compensated depending on whether heuristics and/or GPS/INS loose coupling are used, as shown in equation 21. The process noise and measurement noise were tuned to optimize estimator performance.

$${}^B\vec{a}_{CG/I,comp} = {}^B\vec{a}_{CG/I} - {}^B\vec{a}_{bias,heur} - {}^B\vec{a}_{bias,GPSI} \tag{21}$$

3. Results

3.1 Experimental Setup

The performance of this algorithm was assessed with experimental data from guided flights of a canard-controlled 120-mm mortar. The firing range (figure 3) featured the launcher and gun crew as well as state-of-the-art instrumentation such as high-speed photography, tracking radar, differential GPS survey, telemetry data receivers, and transducers for monitoring tube pressure during gun launch.

Figure 3. Experimental firing range setup (top) and projectile (bottom).

The projectile (shown in figure 3) was instrumented with triaxial accelerometers, triaxial angular rate sensors and a GPS receiver equipped with upfinding capability for projectile roll angle estimation. The accelerometers were not calibrated pre-flight, and the angular rate sensors were calibrated prior to the flights for bias, scale factor, and misalignment.

The control action (canard amplitude and direction) began 14 s into flight and was obtained from onboard measurements and fed into the algorithm. Attitude was estimated using GPS, which was available starting at ~8 s time of flight. Comparing the radar- and GPS-derived pitch and yaw attitude in figure 4 illustrates the typical error associated with using the real-time GPS data for attitude.

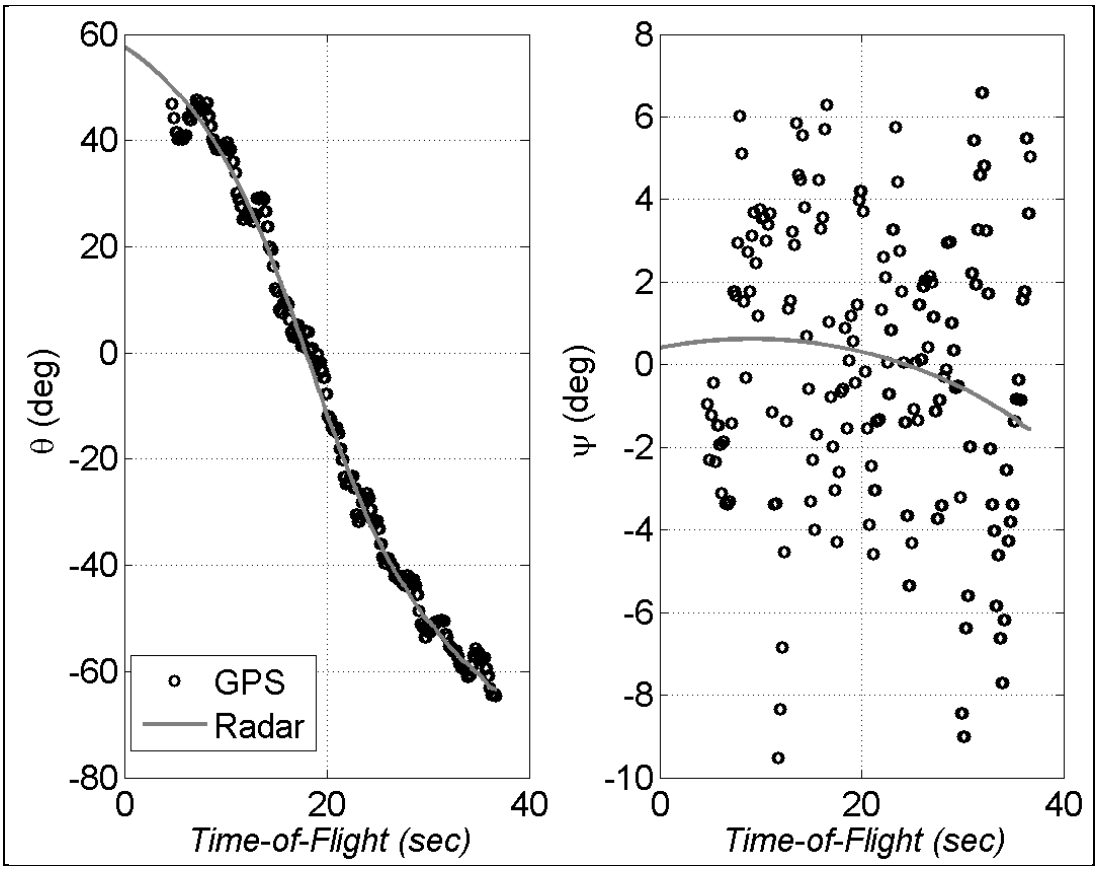

Figure 4. Experimental pitch and yaw angles from radar and GPS.

Tracking radar was used as the truth measure of position and velocity to enable assessment of algorithm performance. The uncertainty in the radar data may be quantified by comparing the impact location from survey and radar. The projectile impacted ~4 km from the gun. Radar impact agreed to within 15.55 m of the surveyed impact location. The survey location using differential GPS has ~0.01-m error. Radar position accuracy degrades with distance since the signal-to-noise ratio of the radar typically decreases with distance and assuming constant azimuth and elevation angle errors of the radar tracking antenna result in a larger position error with distance.

The radar-derived position of the projectile is given in figure 5. The *z*-axis has been flipped from the definition in figure 2 to view the data in a more reasonable manner. The round flew almost 4 km and reached over 1.5 km in altitude in about 40 s time of flight. Examination of the *y*-position shows that the projectile drifted over 20 m off the gun-target line prior to maneuvering to the target.

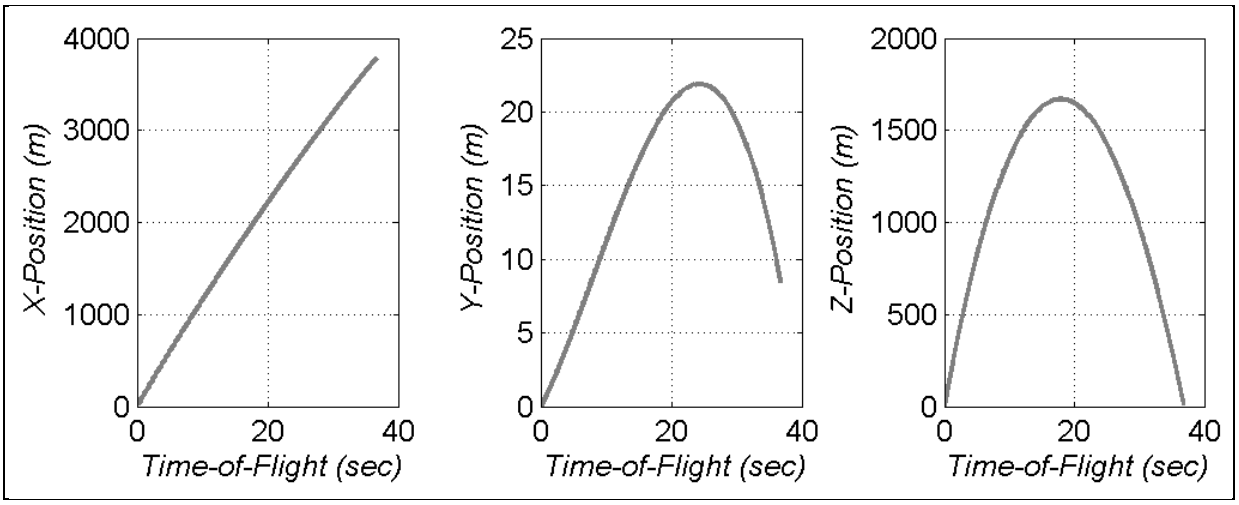

Figure 5. Experimental trajectory from radar.

3.2 Experimental Results

The estimator was evaluated with the experimental data for a few different cases. Raw IMU data were put through the measurement equations (i.e., no filtering) to evaluate the feasibility of applying pure dead reckoning using low-cost sensors to the high dynamic projectile environment. The next case was the EKF algorithm performed on the IMU data without the heuristic or loose coupling options enabled. Estimation was then undertaken using the heuristics. Finally, both the heuristics and the loose coupling were turned on. None of the cases shown for the experiments used GPS directly in the state estimation. GPS was only used to estimate attitude and IMU parameters.

The root-sum-square (RSS) error between the estimator and the radar was used as the metric to infer algorithm performance. RSS position error for the different cases is presented in figure 6. Recall that GPS data required for attitude are unavailable until almost 8 s into flight; therefore, estimation begins at this time and continues until target impact.

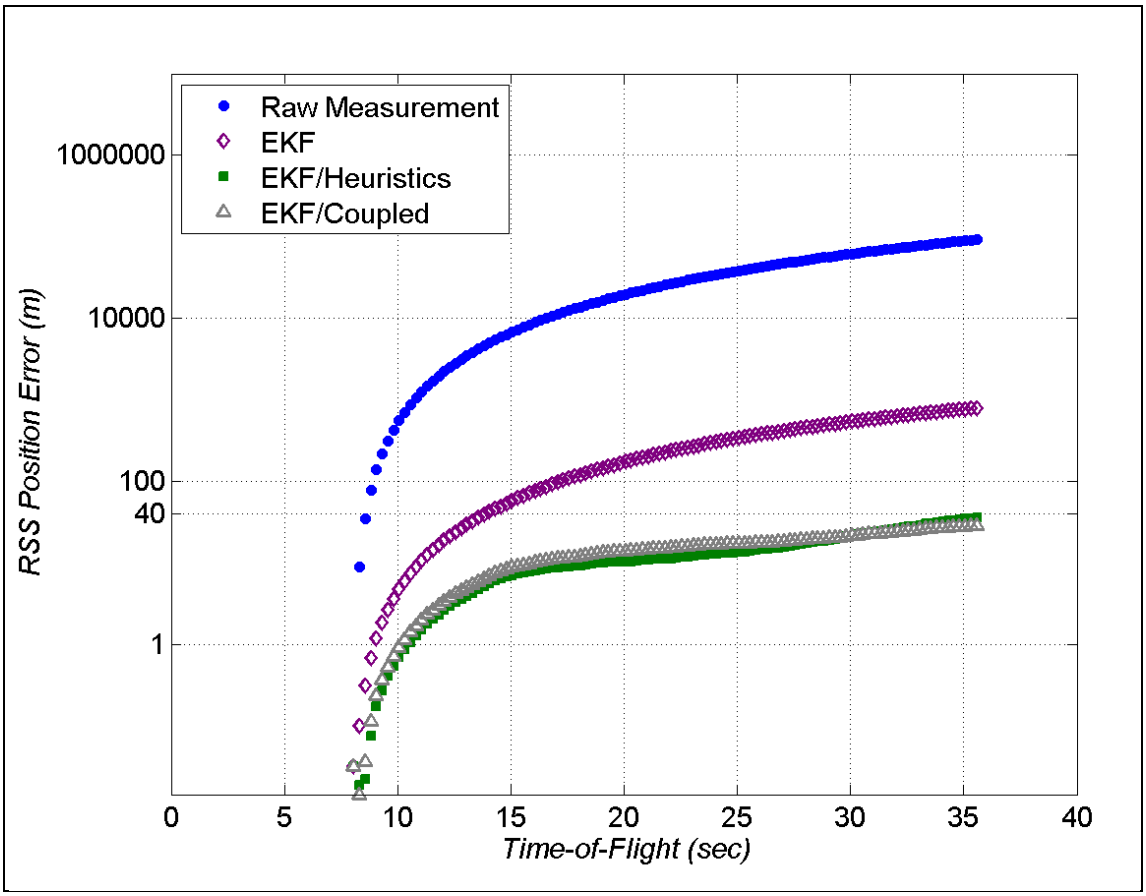

Figure 6. Position errors from experiments.

Direct integration of the raw IMU output is clearly useless in this application. The position error grows to over 100,000 m by impact. Blending the measurements with the flight dynamic model in the EKF improves position estimates over the measurement-only case. Ballistic CEP of these weapon systems, however, is often better than the ~800-m error of the EKF case at impact. Enabling the heuristic parameter in the EKF algorithm drastically reduces position error to less than 40 m at the end of the experimental flight. Using flight dynamic theory to compensate the IMU signal post-launch improves navigation performance. Indeed, loose coupling does not benefit the position solution much over the EKF with the heuristic parameter as the final position is only 5 m closer to the truth value.

The manner in which the heuristic algorithm improves the position estimate is illustrated in figures 7 and 8. Components of the body acceleration without gravity are presented across the top of figure 7. The bottom portion of the figure is a zoomed in view of the axial component.

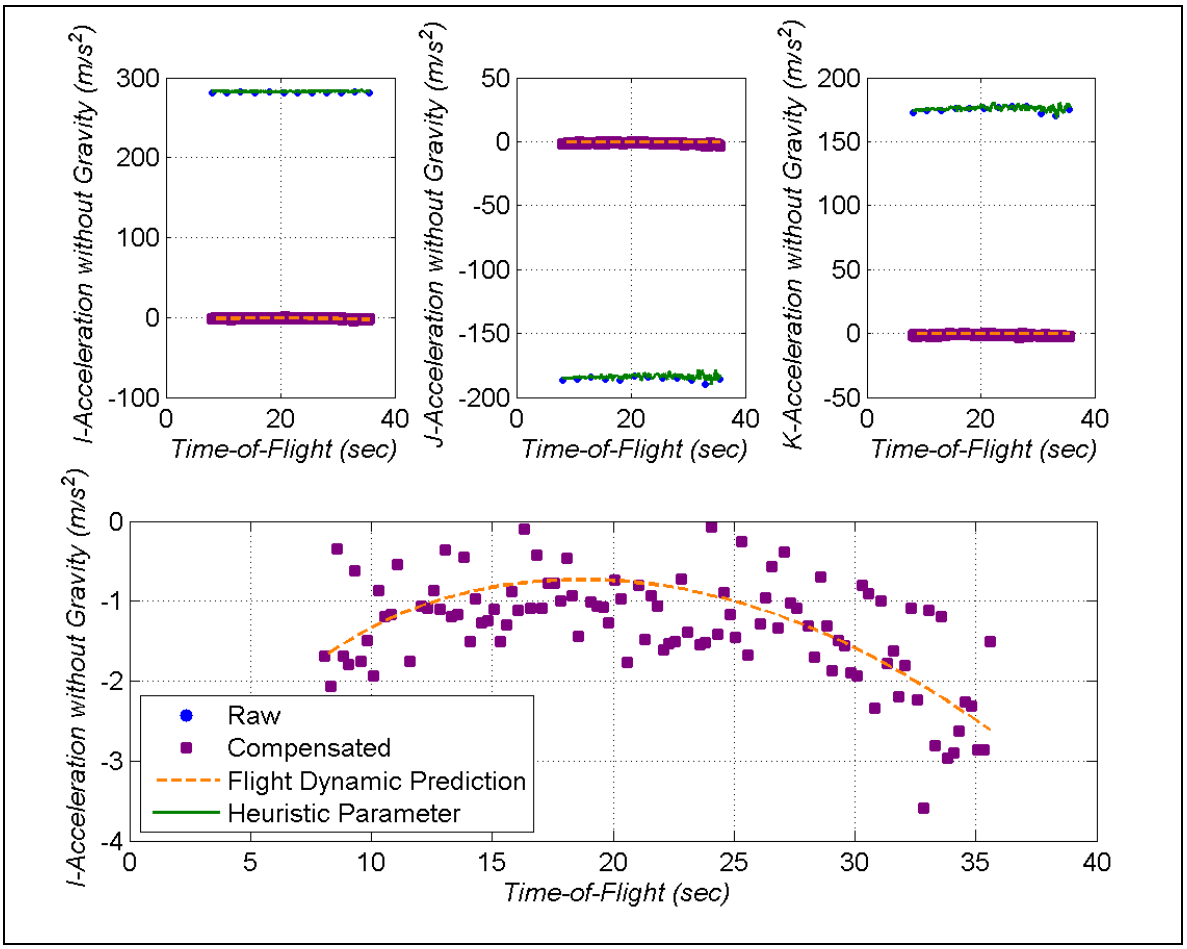

Figure 7. Body acceleration components from experiments (EKF with heuristics).

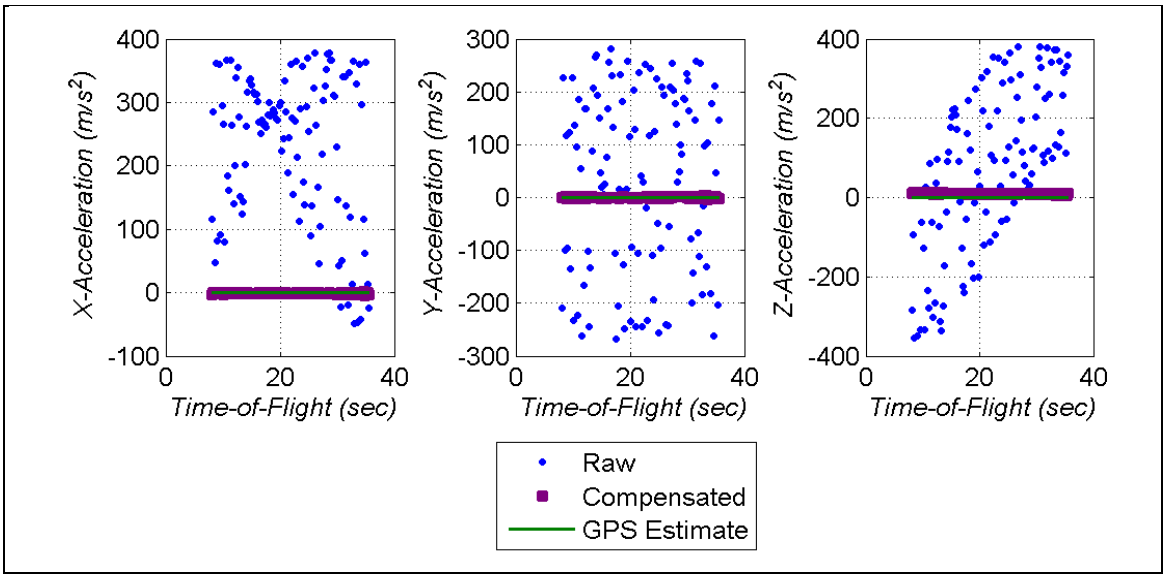

Figure 8. Inertial acceleration components from experiments (EKF with heuristics).

The raw IMU data (obtained through equations 6 and 7) demonstrates a bias error of ~20–30 Gs depending on the axis. While clouded by errors, the pertinent information is included in the measurement. The zoomed in portion of the figure shows the axial component of the flight dynamic predictions of the IMU signal varying 1–2 Gs over the course of the flight. Comparing the measurement with the prediction and smoothing, the difference produces the heuristic parameter magnitude in the figure. Raw measurements are close to the heuristic parameter. The compensated values in the figure result from subtracting the raw measurement from the heuristic parameter. Note how closely the compensated values match the flight dynamic prediction in the zoomed in view of the axial component.

The effect of the heuristic parameter on the inertial acceleration is given in figure 8. Large bias values in the raw measurement body accelerations of figure 7 produce widely varying inertial acceleration components over the course of the flight due to the transformation matrix. The inertial acceleration compensated with the heuristic algorithm produce reasonable, smoothly varying values, which also agree with the smoothed GPS estimates. Differentiating the GPS velocity to yield acceleration amplifies the noise content.

Limited experimental results suggest that, for time of flights of interest to the gun-launched guided projectile community, the EKF algorithm using heuristics with low-cost sensors provides useful navigation information.

3.3 Simulation Setup

In order to evaluate the algorithm under a stochastically significant scenario, models of the system were developed and simulations were performed. A 6DOF model was built of the experimental guided system along with models of the uncertainty in the flight (mass properties, aerodynamics, launch conditions, control mechanism, and atmosphere) and measurements (sensors and attitude estimates). States of the 6DOF were used as truth to quantify algorithm performance. Conditions of the simulation were similar to the experiments. Monte Carlo analysis was undertaken with 500 repetitions of each case.

3.4 Sensor Models

Output of the 6DOF was used to form sensor signals. Truth states of body acceleration, attitude, body angular velocity, and body angular acceleration were corrupted with bias, scale factor, misalignment, and misposition errors for the accelerometers as shown in equation 22. For both accelerometers and gyroscopes, the turn-on bias is initialized at the beginning of each flight using a turn-on standard deviation and norm of zero. The drift is also initialized at the beginning of each flight, and it is additive so that each time step is the previous drift plus the newly calculated drift parameter.

$$
{}^{B}\vec{a}_{A/I} = \vec{S}^{a}\vec{T}_{B/A}\left[\begin{array}{l}\left(\dfrac{{}^{B}\partial\vec{v}_{CG/I}}{\partial t} - \vec{T}_{I/B}\vec{g}\right) + \vec{\alpha}_{B/I}\times\vec{r}_{CG\to A} + \vec{\omega}_{B/I}\times\left(\vec{\omega}_{B/I}\times\vec{r}_{CG\to A}\right) + {}^{B}\vec{a}_{turn\text{–}on} \\ + {}^{B}\vec{a}_{drift,k-1} + \sigma^{a}_{drift}\cdot N(0,1) + \sigma^{a}_{noise}\cdot N(0,1)\end{array}\right] \tag{22}
$$

Bias, scale factor, and misalignment were added to the 6DOF body angular rate for the gyroscopes, as given in equation 23. The bias error for the accelerometers and gyroscopes includes turn-on and in-run terms.

$$
\vec{\omega}_{B/I} = \vec{S}^{g}\vec{T}_{B/G}\left[\vec{\omega}_{B/I} + \vec{\omega}_{B/I,turn\text{–}on} + \vec{\omega}_{B/I,drift,k-1} + \sigma^{g}_{drift}\cdot N(0,1) + \sigma^{g}_{noise}\cdot N(0,1)\right] \tag{23}
$$

3.5 Simulation Parameters

The error budget for the uncertainty in flight and measurements used in the Monte Carlo simulations is given in table 1. These error budgets are based on laboratory measurements and gun firings of instrumented projectiles. The low-cost MEMs sensors have large error magnitudes.

Table 1. Simulation error budget.

	Parameter	**Error (1σ)**
Accelerometer	$\vec{r}_{CG\to A}$	0.5 mm
	$\vec{S}^{a}$	1% full scale value
	$\vec{T}_{B/A}$	0.5°
	$\sigma^{a}_{turn\text{–}on}$	16,000 mG
	σ_{drift}	4 mG
	σ^{a}_{noise}	26 mG
Gyroscope	$\vec{S}^{g}$	2.1% full scale value
	$\vec{T}_{B/G}$	0.5°
	$\sigma^{g}_{turn\text{–}on}$	44,685°/h
	σ^{g}_{drift}	22°/h
	σ^{g}_{noise}	2.2°/h
Flight	m	0.001 kg
	C_{D}	1%
	$C^{B}_{L\alpha}, C^{C}_{L\alpha}$	5%
	d	0.001 m

3.6 Simulation Results

Simulations were conducted to validate modeling and simulation and examine the effect of attitude uncertainty, the number of IMU arrays, heuristics, and GPS availability on the state estimation algorithm. The nominal error budget was used unless otherwise stated. The nominal attitude error was 5° 1σ bias error and 10° 1σ random error (both errors normally distributed). The magnitude of these attitude errors is reasonable using previously developed algorithms which employ low-cost, gun-hardened sensors (*28–31*).

3.7 Validation With Raw Measurements

In order to validate the sensor model and error budget, simulated raw IMU data were put through the measurement equations (i.e., no filtering). Position errors from these Monte Carlo simulations are on the same order of magnitude as the experimental result as shown in figure 9, which indicates that sensor modeling and the error budget are reasonable.

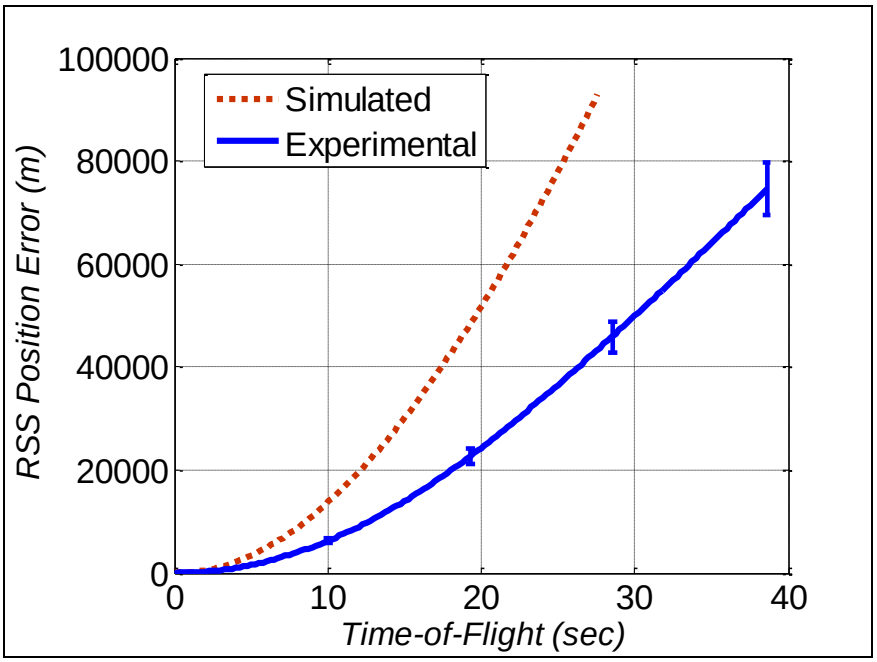

Figure 9. Position errors from simulation (with 95% confidence interval error bars) and experiment with raw IMU measurements.

3.8 Attitude Uncertainty

The effect of attitude uncertainty on the algorithm was assessed by varying the attitude errors in the Monte Carlo simulations. The 1σ bias error was adjusted from 0°–10° and the 1σ random error was adjusted from 0°–20° (both errors normally distributed). The resulting position error using the EKF algorithm with heuristics is shown in figure 10. Using heuristics, the algorithm is tolerant to attitude error due to the manner in which the flight dynamics are heavily weighted in the estimate.

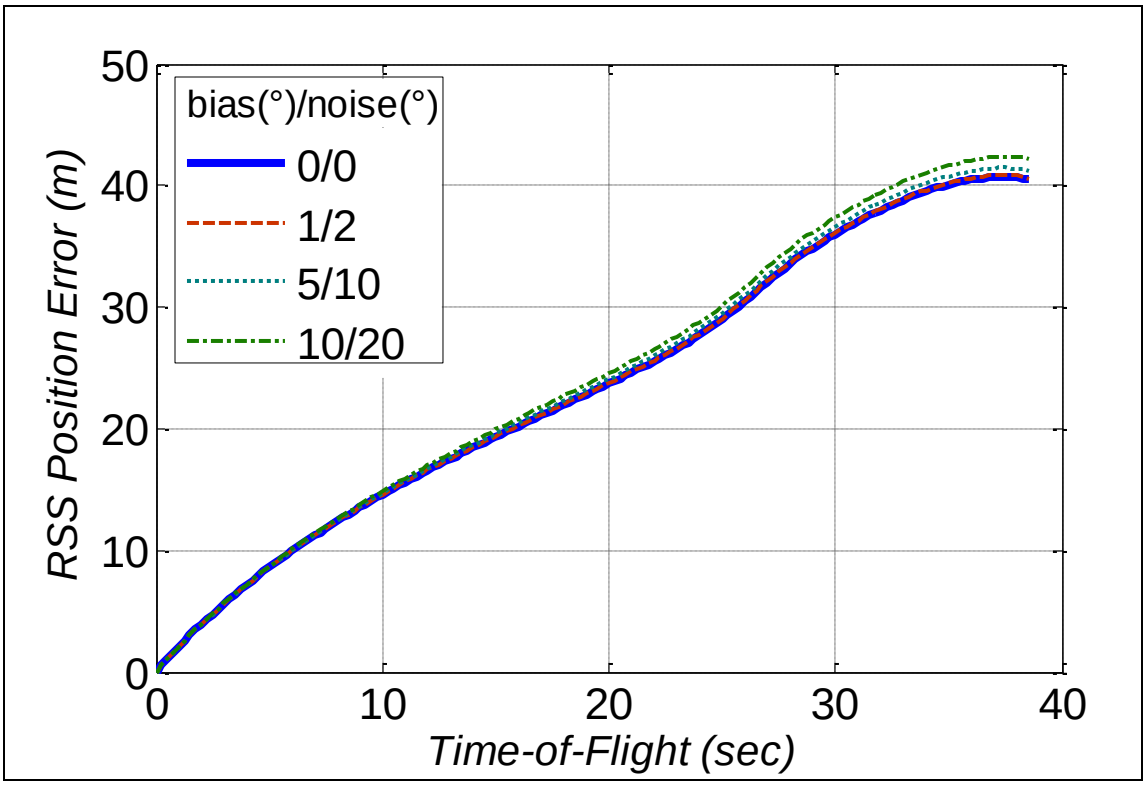

Figure 10. Position errors from simulation varying attitude error (EKF with heuristics).

3.9 Number of IMU Arrays

As previously demonstrated, a MEMs IMU has significant error sources. Bias is an important error source, which often cannot be observed for the purpose of compensation (*28–31*). One way to compensate for sensor biases is to use multiple IMU arrays and to average them. By averaging multiple IMU arrays, biases and other sources of errors may be mitigated.

Simulations were conducted to assess the relationship between the number of MEMs IMU arrays and the position error. Figure 11 shows position errors for the EKF algorithm without heuristics or loose coupling from the Monte Carlo simulations with the number of arrays varying from 1 to 100. These results suggest that increasing the number of arrays has a large effect on the position estimate if heuristics and loose coupling are not included in the algorithm. With 1 array, the final position error is at 126 m. Final position error falls by 61% (48 m) with 10 arrays and subsequently drops to 75% (31 m) if 100 arrays are used. Although large arrays may not be feasible especially in small-caliber projectiles, MEMs devices continue to decrease in size (e.g., multiple sensors on a chip) and cost and increase in performance. Additionally, future precision guided munition concepts could distribute sensors and electronics throughout the body as an integrated part of subsystems such as the warhead.

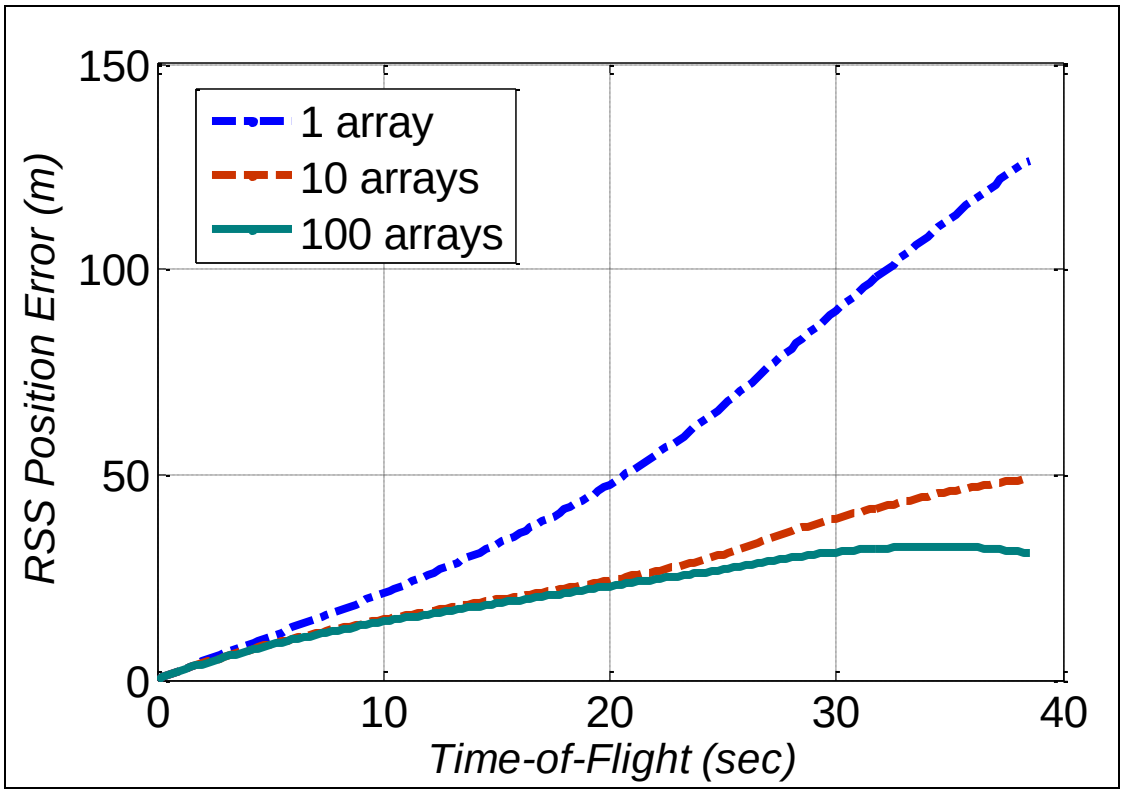

Figure 11. Position errors from simulation varying the number of IMU arrays.

3.10 Heuristics

Experiments indicated that using flight dynamic heuristics in the EKF improved the position estimates by over an order of magnitude. Monte Carlo simulations further support this finding. Figure 12 shows the position errors from the simulation for the EKF without and with the heuristics enabled. Using heuristics to compensate the raw measurements decreases the position error by 66%. Position errors of the algorithm with heuristics are similar in magnitude to GPS for about 10 s and the error growth is such that after 10 s the navigation solution of this algorithm would likely improve the ballistic system CEP.

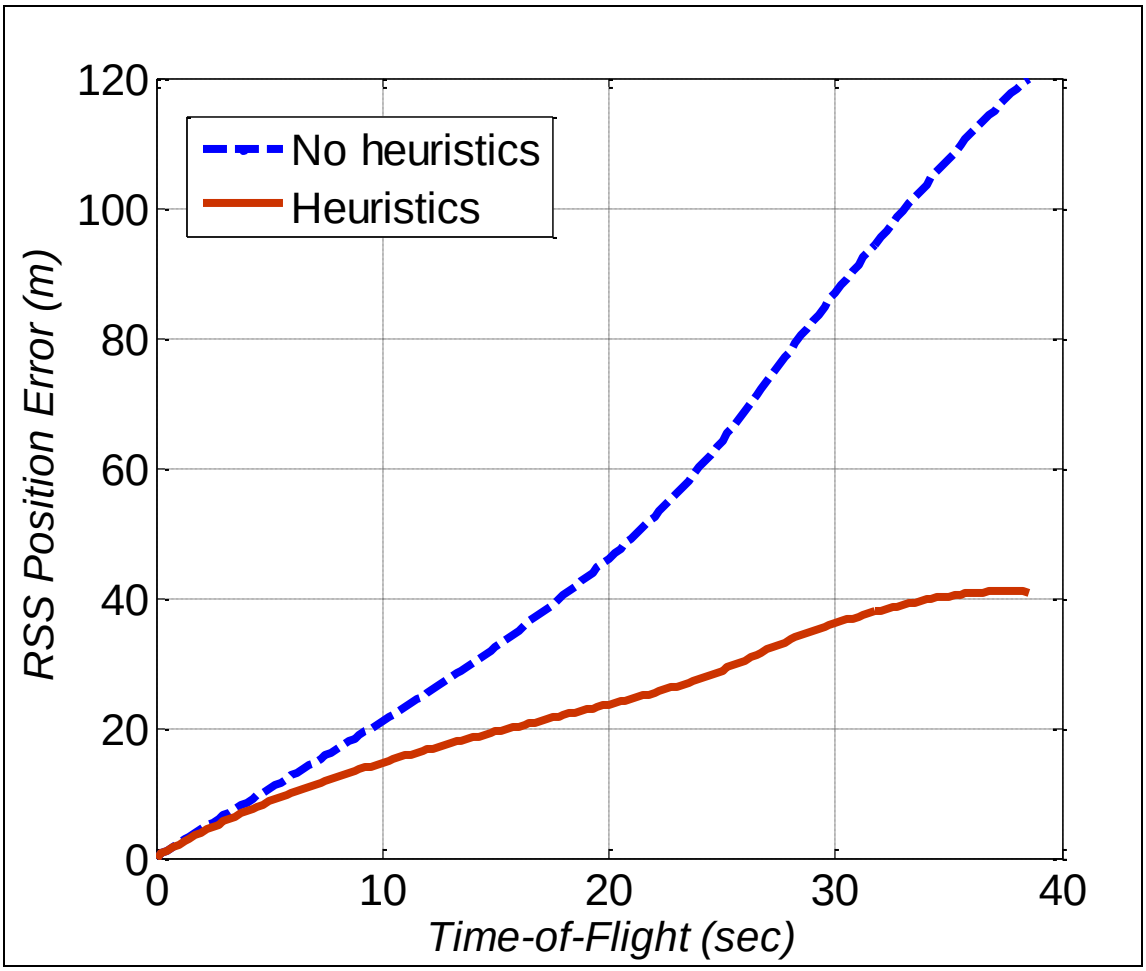

Figure 12. Position errors from simulation considering the effect of heuristics.

3.11 Loosely coupled GPS/INS

GPS can contribute to the state estimate by calibrating the IMU post-launch; however, GPS may be lost in flight due to terrain or jamming. The effect of GPS availability on the GPS/INS parameter and ultimately the position error was evaluated in simulation. Cases were run where the GPS was always present, lost at 10, 20, and 30 s. Monte Carlo simulation of the EKF algorithm with GPS/INS (no heuristics) was executed for these cases and the results are given in figure 13. Compensating the IMU measurement with the GPS/INS parameter improved the position errors over the EKF or EKF with heuristics. Moreover, the algorithm was insensitive to the amount of time for which GPS data were available before apogee. There is only about a 35-m difference in the final position error between losing GPS at 10 s and having GPS throughout the entire flight. The increase in error when GPS is lost at 20 s is due to maneuvers. Trading off between estimator smoothness and accuracy was performed by tuning the measurement covariance matrix as a function of flight time to rely more on GPS later in the flight.

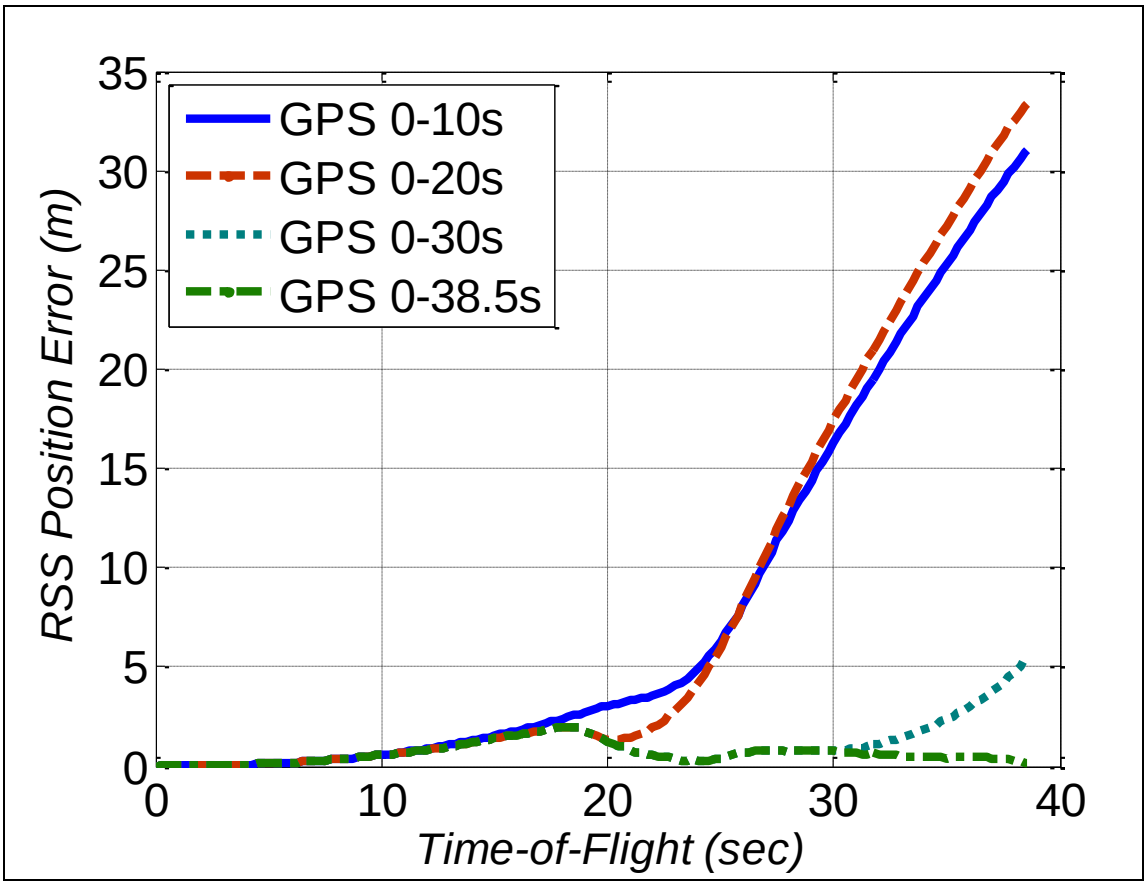

Figure 13. Position errors from simulation considering the effect of loose coupling without heuristics.

4. Conclusions

Improving the precision of gun-launched munitions is an active area of research for the U.S. Army. Affordability, survivability, and fast dynamics are among the technical barriers to achieving precision munitions. Ballistic launch and flight is inherently effective at delivering lethal payloads. Often, projectile guidance systems need only nudge the projectile trajectory to ensure that the target is within the lethal area of the warhead.

Navigating the projectile in space is a critical element of any guided system. This report is unique in examining the minimal navigation technologies for decreasing the system CEP at low cost. Projectile flight dynamics are used in a novel manner in the state and heuristic parameter estimation to meet these goals.

The algorithm for estimating position and velocity was shown. The PMC flight dynamic model was built into an EKF, which used IMU and attitude (and GPS if available) data. MAFs for heuristic and GPS/INS bias parameters were applied to compensate for measurement errors.

Experimental flights of a guided mortar system were used to evaluate the algorithm performance. Comparing ground-truth radar data with algorithm output revealed many interesting findings. Uncompensated dead reckoning with the raw measurements produces very large position errors due to high MEMs device error sources. Blending these measurements with the PMC dynamic model in the EKF improves the position errors by orders of magnitude. Including the unique flight dynamic heuristic in the algorithm improved the position errors to less than 40 m by the end of the flight. Assuming GPS availability and augmenting the algorithm with the GPS/INS parameter enhances results over the EKF with heuristic case. The limited experimental results suggest the algorithm can improve system CEP with low cost and computational throughput.

Monte Carlo simulations support the experiments. The heuristic parameter provides tactically useful navigation errors by compensating the measurements with known flight dynamic information. The algorithm was intolerant to the error in attitude estimates. A 10-array IMU decreases position errors by about a factor of two over a single array; adding up to 100 arrays does not noticeably improve accuracy over the 10-array case. The duration of GPS availability was important when maneuvering as GPS data were necessary for the MAF to satisfactorily determine the GPS/INS bias parameter. These results demonstrate the value in using known flight dynamic characteristics in the position estimation algorithm to mitigate errors in low-cost sensors to meet threshold objectives in system accuracy.

5. References

1. Fresconi, F. E. Guidance and Control of a Projectile with Reduced Sensor and Actuator Requirements. *AIAA Journal of Guidance, Control, and Dynamics* **November–December 2011**, *34* (6), 1757–1766.
2. Morrison, P. H.; Ambernston, D. S. Guidance and Control of Cannon-Launched Guided Projectile. *Journal of Spacecraft and Rockets* **1977**, *14* (6), 328–334.
3. Davis, B.; Malejko, G.; Dorhn, R.; Owens, S.; Harkins, T.; Bischer, G. Addressing the Challenges of a Thruster-Based Precision Guided Mortar Munitions With the Use of Embedded Telemetry Instrumentation. *ITEA Journal* **2009**, *30*, 117–125.
4. Moorhead, J. S. Precision Guided Kits (PGKs): Improving the Accuracy of Conventional Cannon Rounds. *Field Artillery* **January-February 2007**, 31–33.
5. Grubb, N. D.; Belcher, M. W. Excalibur: New Precision Engagement Asset in the Warfight. *Fires* **October-December 2008**, 14–15.
6. Wells, L. L. The Projectile GRAM SAASM for ERGM and Excalibur. In *IEEE/ION Position, Location and Navigation Symposium*, San Diego, CA, 2000.
7. Grace, J. GPS Guidance System Increases Projectile Accuracy. *IEEE Aerospace and Electronic Systems Magazine* **2000**, *15* (6), 15–17.
8. Fresconi, F.; Brown, T.; Celmins, I.; DeSpirito, J.; Ilg, M.; Maley, J.; Magnotti, P.; Scanlan, A.; Stout, C.; Vazquez, E. Very Affordable Precision Projectile System and Flight Experiments. In *Army Science Conference*, Orlando, FL, 2010.
9. Savage, P. G. *Strapdown Analytics*; Strapdown Associates: Maple Plain, MN, 2000.
10. Godha, S.; Cannon, M. GPS/MEMS INS Integrated System for Navigation in Urban Areas. *GPS Solutions* **2007**, *11*, 193–203.
11. Skog, I.; Handel, P. In-Car Positioning and Navigation Technologies - A Survey. *IEEE Transactions on Intelligent Transportation Systems* **2009**, *10* (1), 4–21.
12. Grewal, M.; Weill, L.; Andrew, A. *Global Positioning Systems, Inertial Navigation, and Integration*; 2nd ed.; Wiley-Interscience: New York, 2007.
13. D'Amico, W. P. Telemetry Sytems and Electric Gun Projectiles. *IEEE Transactions on Magnetics* **2001**, *37* (1), 343–346.

14. Brown, T. G.; Davis, B.; Hepner, D.; Faust, J.; Myers, C.; Muller, P.; Harkins, T.; Hollis, M.; Miller, C.; Placzankis, B. Strap-Down Microelectromechanical Sensors for High-G Munition Applications. *IEEE Transactions on Magnetics* **2001**, *37* (1), 336–342.

15. Barbour, N.; Schmidt, G. Inertial Sensor Technology Trends. *IEEE Sensors Journal* **2001**, *1* (4), 332–339.

16. Habibi, S.; Cooper, S. J.; Stauffer, J. M. Gun Hard Inertial Measurement Unit Based on MEMS Capacitive Accelerometer and Rate Sensor. In *IEEE/ION Position, Location and Navigation Symposium*, Monterey, CA, 2008.

17. Sheard, K.; Scaysbrook, I.; Cox, D. MEMS Sensor and Integrated Navigation Technology for Precision Guidance. In *IEEE/ION Position, Location and Navigation Symposium*, Monterey, CA, 2008.

18. Scaysbrook, I. W.; Cooper, S. J.; Whitley, E. T. A Miniature, Gun-Hard MEMS IMU for Guided Projectiles, Rockets and Missiles. In *IEEE/ION Position, Location and Navigation Symposium*, Monterey, CA, 2004.

19. Mermagen, W. H. High-g Resistant Electronic Fuse of Projectile Payloads. *Journal of Spacecraft and Rockets* **1971**, *8* (8), 900–903.

20. Murphy, C. *Free Flight of Symmetric Missiles*; U.S. Army Ballistics Research Laboratory: Aberdeen Proving Ground, MD, 1963.

21. Nicolaides, J. *On Missile Flight Dynamics*; Catholic University of America: Washington DC, 1963.

22. Cooper, G.; Costello, M.; Fresconi, F. Flight Stability of Asymmetric Projectiles with Control Mechanisms. *Journal of Spacecraft and Rockets* **2012**, *49* (1), 130–135.

23. Fresconi, F.; Harkins, T. Experimental Flight Characterization of Asymmetric and Manuevering Projectiles from Elevated Gun Firings. *Journal of Spacecraft and Rockets*, accepted 18 January, 2012.

24. Fresconi, F.; Celmins, I.; Fairfax, L. Optimal Parameters for Maneuverability of Affordable Precision Munitions, in AIAA Aerospace Sciences Meeting Proceedings, Orlando, FL, 2012.

25. Fresconi, F.; Cooper, G.; Costello, M. Practical Assessment of Real-Time Impact Point Estimators for Smart Weapons. *Journal of Aerospace Engineering* **2011**, *24* (1), 1–11.

26. Koifman, M.; Bar-Itzhack, I. Inertial Navigation System Aided by Aircraft Dynamics. *IEEE Transactions on Control Systems Technology* **1999**, *7* (4), 487–493.

27. Burchett, B. T.; Costello, M. F. Specialized Kalman Filtering for Guided Projectiles. In *39th AIAA Aerospace Sciences Meeting & Exhibit*, Reno, NV, 2001.

28. Rogers, J.; Costello, M.; Hepner, D. Roll Orientation Estimator for Smart Projectiles Using Thermopile Sensors. *AIAA Journal of Guidance, Control, and Dynamics* **2011**, *34* (3), 688–697.

29. Maley, J. Roll Orientation from Commercial-Off-The-Shelf (COTS) Sensors in the Presence of Inductive Actuators. In *Institute of Navigation Joint Navigation Conference*, Colorado Springs, CO, 2010.

30. Rogers, J.; Costello, M.; Harkins, T.; Hamaoui, M. Effective Use of Magnetometer Feedback for Smart Projectile Applications. *Navigation*, accepted for publication.

31. Rogers, J.; Costello, M.; Harkins, T.; Hamaoui, M. A Low-Cost Orientation Estimator for Smart Projectiles Using Magnetometers and Thermopiles. *Navigation*, accepted for publication.

32. Kaplan, E. D.; Hegarty, C. J. *Understanding GPS Principals and Applications*; 2nd ed.; Artech House: Norwood, MA, 2006.

33. Simon, D. *Optimal State Estimation: Kalman, H-infinity, and Nonlinear Approaches*; Wiley-Interscience: Hoboken, NJ, 2008.

34. Savage, P. A Unified Mathematical Framework for Strapdown Algorithm Design. *Journal of Guidance, Control and Dynamics* **2006**, *29* (2), 237–249.

35. Fresconi, F.; Cooper, G. R.; Celmins, I.; DeSpirito, J.; Costello, M. Flight Mechanics of a Novel Spin-Stabilized Projectile Concept. *Journal of Aerospace Engineering* **2011**, *226 Part G*, 327–340.

List of Symbols, Abbreviations, and Acronyms

6DOF	six degree-of-freedom
CEP	circular error probable
CG	center of gravity
EKF	extended Kalman filter
GPS	global positioning system
IMU	inertial measurement units
INS	inertial navigation system
MAF	moving average filter
MEMS	micro-electromechanical
PMC	point-mass with control
RSS	root-sum-square
${}^{I}\vec{a}_{CG/I,GPS}$	acceleration at CG with respect to inertial frame according to GPS
${}^{B}\vec{a}_{CG/I}$	acceleration at CG with respect to inertial frame in body coordinates
${}^{I}\vec{a}_{CG/I}$	acceleration at CG with respect to inertial frame in inertial coordinates
${}^{B}\vec{a}_{A/B}$	acceleration at point A with respect to body in body coordinates
${}^{B}\vec{a}_{A/I}$	acceleration at point a with respect to inertial frame in body coordinates
$\vec{g}$	acceleration due to gravity in inertial frame
$\frac{\partial \vec{v}_{CG/I}}{\partial t}$	acceleration of the CG with respect to inertial frame in body coordinates
${}^{B}\vec{a}_{drift,k-1}$	accelerometer drift bias at time *k*-1
σ^{a}_{drift}	accelerometer drift bias standard deviation
$\vec{T}_{B/A}$	accelerometer misalignment transformation
${}^{B}\vec{a}_{turn-on}$	accelerometer turn-on bias

$\sigma_{turn-on}$	accelerometer turn-on bias standard deviation
σ^{a}_{noise}	accelerometer white noise standard deviation
C_D	aerodynamic drag coefficient
ρ	air density
$z, \dot{z}, \ddot{z}$	altitude position, velocity and acceleration in inertial coordinates
$\vec{\alpha}_{B/I}$	angular acceleration of body with respect to inertial frame
$\vec{\omega}_{B/I}$	angular velocity of body with respect to inertial frame
L_B	body lift force
$C^{B}{}_{L\alpha}$	body lift force coefficient
δ	canard deflection amplitude
ϕ_{CAN}	canard deflection roll orientation
L_{CAN}	canard lift force
$C^{C}{}_{L\alpha}$	canard lift force coefficient
${}^{B}\vec{a}_{CG/I,comp}$	compensated acceleration of CG with respect to I in body frame
$y, \dot{y}, \ddot{y}$	crossrange position, velocity and acceleration in inertial coordinates
$x, \dot{x}, \ddot{x}$	downrange position, velocity and acceleration in inertial coordinates
P_k	error covariance at time *k*
dt_{GPS}	GPS update rate
${}^{B}\vec{a}_{bias,GPSI,k}$	GPS/INS loosely coupled acceleration bias at time step *k*
${}^{B}\vec{a}_{bias,GPSI}$	GPS/INS loosely coupled acceleration bias, smoothed
$\vec{\omega}_{B/I,drift,k-1}$	gyroscope drift bias at time *k*-1
σ^{g}_{drift}	gyroscope drift bias standard deviation
$\vec{T}_{B/G}$	gyroscope misalignment transformation
$\vec{\omega}_{B/I,turn-on}$	gyroscope turn-on bias

$\sigma^{g}_{turn-on}$	gyroscope turn-on bias standard deviation
σ^{g}_{noise}	gyroscope white noise standard deviation
${}^{B}\vec{a}_{bias,heur,k}$	heuristic acceleration bias at time step *k*
${}^{B}\vec{a}_{bias,heur}$	heuristic acceleration bias, smoothed
${}^{B}\vec{a}_{CG/I,heur}$	heuristic acceleration estimate
ρ_{heur}	heuristic fading memory coefficient
dt	INS update rate
K_{ik}	Kalman gain of measurement *i* at time *k*
ρ_{GPSI}	loosely coupled GPS/INS fading memory coefficient
R_{ik}	measurement covariance of measurement *i* at time *k*
y_{ik}	measurement *i* at time *k*
Q_{k-1}	model covariance at time *k*-1
$\vec{r}_{CG\to A}$	moment arm from center of gravity to INS location
$N(0,1)$	normally distributed random number, 0 mean, 1 standard deviation
${}^{I}\vec{x}_{k}$	position in inertial frame at time *k*
α	projectile angle-of-attack
d	projectile diameter
m	projectile mass
ϕ,θ,ψ	projectile roll, pitch and yaw attitude
$\vec{S}^{a},\vec{S}^{g}$	scale factor for accelerometer, gyroscope
X_{k}	state at time *k*
A_{k-1}	system dynamics matrix at time *k*-1
V_{∞}	total air velocity
$\vec{T}_{B/I},\vec{T}_{I/B}$	transformation matrix from body to inertial, inertial to body coordinates
${}^{I}\vec{v}_{GPS,k}$	velocity from GPS at time *k*

$^{I}\vec{v}_{k}$	velocity in inertial frame at time k
I	identity matrix

NO. OF COPIES	ORGANIZATION
1 (PDF only)	DEFENSE TECHNICAL INFORMATION CTR DTIC OCA 8725 JOHN J KINGMAN RD STE 0944 FORT BELVOIR VA 22060-6218
1	DIRECTOR US ARMY RESEARCH LAB IMNE ALC HRR 2800 POWDER MILL RD ADELPHI MD 20783-1197
1	DIRECTOR US ARMY RESEARCH LAB RDRL CIO LL 2800 POWDER MILL RD ADELPHI MD 20783-1197
1	DIRECTOR US ARMY RESEARCH LAB RDRL CIO LT 2800 POWDER MILL RD ADELPHI MD 20783-1197
1	DIRECTOR US ARMY RESEARCH LAB RDRL D 2800 POWDER MILL RD ADELPHI MD 20783-1197

NO. OF COPIES	ORGANIZATION
7	RDECOM ARDEC RDAR MEF E D CARLUCCI M HOLLIS C STOUT A SANCHEZ R HOOKE J MURNANE T RECCHIA BLDG 94 PICATINNY ARSENAL NJ 07806-5000
9	RDECOM ARDEC RDAR MEF S D PANHORST G MINER N GRAY R FULLERTON B DEFRANCO M MARSH P FERLAZZO D PASCUA J ROMANO BLDG 94 PICATINNY ARSENAL NJ 07806-5000
7	RDECOM ARDEC RDAR MEM C D NGUYEN R GORMAN D CIMORELLI K SANTANGELO D DEMELLA P MAGNOTTI A LICHTENBERG-SCANLAN BLDG 94 PICATINNY ARSENAL NJ 07806-5000
2	RDECOM ARDEC RDAR MEM M C MOEHRINGER J TRAVAILLE BLDG 94 PICATINNY ARSENAL NJ 07806-5000
4	RDECOM ARDEC RDAR MEM A E VAZQUEZ G MALEJKO W KOENIG S CHUNG BLDG 94S PICATINNY ARSENAL NJ 07806-5000

NO. OF COPIES	ORGANIZATION
1	RDECOM ARDEC RDAR MEM A J GRAU BLDG 94 PICATINNY ARSENAL NJ 07806-5000
3	RDECOM ARDEC RDAR MEF I R GRANITZKI J CHOI L VO BLDG 95 PICATINNY ARSENAL NJ 07806
1	RDECOM ARDEC RDAR MEM C M LUCIANO BLDG 65S PICATINNY ARSENAL NJ 07806
1	US ARMY ARDEC PROPULSION INDIRECT FIRE BR RDAR MEE W J LONGCORE BLDG 382 PICATINNY ARSENAL NJ 07806
1	RDECOM ARDEC RDAR MEF M HOHIL BLDG 407 PICATINNY ARSENAL NJ 07806-5000
4	RDECOM ARDEC AMSRD AMR SG SD J BAUMAN H SAGE S DUNBAR B NOURSE BLDG 5400 REDSTONE ARSENAL AL 35898
1	RDECOM AMRDEC RDMR WDG N B GRANTHAM BLDG 5400 REDSTONE ARSENAL AL 35898
2	PM CAS SFAE AMO CAS R KIEBLER P MANZ BLDG 171 PICATINNY ARSENAL NJ 07806

NO. OF COPIES ORGANIZATION

2 PM CAS
SFAE AMO CAS EX
J MINUS
M BURKE
BLDG 171
PICATINNY ARSENAL NJ 07806

2 PM MORTAR SYS
SFAE AMO CAS MS
P BURKE
G SCHWARTZ
BLDG 162 S
PICATINNY ARSENAL NJ 07806-5000

1 PM MAS
SFAE AMO MAS
C GRASSANO
BLDG 354
PICATINNY ARSENAL NJ 07806

1 PM MAS
SFAE AMO MAS LC
D RIGOGLIOSO
BLDG 354
PICATINNY ARSENAL NJ 07806

1 PM MAS
SFAE AMO MAS SETI
J FOULTZ
BLDG 354
PICATINNY ARSENAL NJ 07806

1 FIRES DEPUTY MGR
EXP MANEUVER WARFARE
OFC OF NAVAL RSRCH
ONR 30
875 N RANDOLPH ST
RM 1155B
ARLINGTON VA 22203

2 NVL SURFC WARFARE CTR
DAHLGREN DIVISION
N COOK
L STEELMAN
G33
6210 TISDALE RD STE 223
DAHLGREN VA 22448-5114

1 ALLIANT TECHSYSTEMS INC
ALLEGANY BALLISTICS LAB
S OWENS
MS WV01 08 BLDG 300 RM 180
210 STATE RTE 956
ROCKET CTR WV 26726-3548

NO. OF COPIES ORGANIZATION

1 SAIC
J NORTHRUP
8500 NORMANDALE LAKE BLVD
STE 1610
BLOOMINGTON MN 55437-3828

1 SAIC
D HALL
1150 FIRST AVE STE 400
KING OF PRUSSIA PA 19406

1 GEN DYNAMICS ST MARKS
H RAINES
PO BOX 222
SAINT MARKS FL 32355-0222

1 GEN DYNAMICS ARM SYS
J TALLEY
128 LAKESIDE AVE
BURLINGTON VT 05401

3 GOODRICH SENS AND INERTIAL SYS
T KELLY
P FRANZ
S ROUEN
100 PANTON RD
VERGENNES, VT 05491

4 BAE ARM SYS DIV
T MELODY
J DYVIK
B GOODELL
O QUORTRUP
4800 E RIVER RD
MINNEAPOLIS MN 55421-1498

1 US ARMY YUMA PROVING GROUND
TEDT YPY MW
M BARRON
301 C STREET
YUMA AZ 85365-9498

1 TRAX INTRNTL CORP
R GIVEN
US ARMY YUMA PROVING GROUND
BLDG 2333
YUMA AZ 85365

1 ARROW TECH ASSOC
W HATHAWAY
1233 SHELBURNE RD
STE D-8
SOUTH BULINGTON VT 05403

NO. OF COPIES ORGANIZATION

1 GEORGIA INST OF TECHLGY
SCHOOL OF AEROSPACE ENG
M COSTELLO
ATLANTA GA 30332

1 TEXAS A&M
SCHOOL OF AEROSPACE ENG
J ROGERS
COLLEGE STATION, TX 77843

ABERDEEN PROVING GROUND

5 COMMANDER
US ARMY TACOM ARDEC
AMSRD AR AEF D
J MATTS
A SOWA
J FONNER
M ANDRIOLO
B NARIZZANO
BLDG 305
APG MD 21005

52 DIR USARL
RDRL WM
P PLOSTINS
RDRL WML
J NEWILL
M ZOLTOSKI
RDRL WML A
W OBERLE
R PEARSON
L STROHM
RDRL WML D
M NUSCA
J SCHMIDT
RDRL WML E
V BHAGWANDIN
I CELMINS

NO. OF COPIES ORGANIZATION

G COOPER
J DESPIRITO
L FAIRFAX (5 CPS)
F FRESCONI (5 CPS)
J GARNER
B GUIDOS
K HEAVY
G OBERLIN
J SAHU
S SILTON
P WEINACHT
RDRL WML F
B ALLIK
F BRANDON
T BROWN
B DAVIS
T HARKINS
D HEPNER
M ILG
G KATULKA
D LYON
J MALEY
R MCGEE
C MILLER
P MULLER
P PEREGINO
D PETRICK
B TOPPER
RDRL WML G
J BENDER
W DRYSDALE
M MINNICINO
RDRL WML H
M FERMER-COKER
R SUMMERS
RDRL WMP F
R BITTING
N GNIAZDOWSKI

INTENTIONALLY LEFT BLANK.